



Effect of nickel doping concentration on structural and magnetic properties of ultrafine diluted magnetic semiconductor ZnO nanoparticles

Prashant K. Sharma*, Ranu K. Dutta, Avinash C. Pandey

Nanophosphor Application Centre, University of Allahabad, Allahabad 211002, India

ARTICLE INFO

Article history:

Received 30 May 2009

Available online 23 June 2009

Keywords:

DMS

Ferromagnetism

VSM

Raman Spectroscopy

ABSTRACT

The ZnO:Ni²⁺ nanoparticles of mean size 2–12 nm were synthesized at room temperature by the simple co-precipitation method. The crystallite structure, morphology and size were determined by X-ray diffraction (XRD) and high-resolution transmission electron microscopy (HRTEM). The wurtzite structure of ZnO gradually degrades with the increasing Ni doping concentration and an additional NiO-associated diffraction peak was observed above 15% of Ni²⁺ doping. The change in magnetic behavior of the nanoparticles of ZnO with varying Ni²⁺ doping concentration was investigated using a vibrating sample magnetometer (VSM). Initially, these nanoparticles showed strong ferromagnetic behavior, however, at higher doping percentage of Ni²⁺, the ferromagnetic behavior was suppressed and paramagnetic nature was observed. The enhanced antiferromagnetic interaction between neighboring Ni–Ni ions suppressed the ferromagnetism at higher doping concentrations of Ni²⁺.

© 2009 Elsevier B.V. All rights reserved.

1. Introduction

In recent years, the scientific community has paid much attention to the synthesis and characterization of II–VI semiconductor materials at nanometer scale, due to their great potential to test fundamental concepts of quantum mechanics [1,2] and because of their key role in various applications such as solid-state lighting devices (LEDs), photonics [3], nanoelectronics [4], optoelectronics and data storage. ZnO is an important II–VI semiconductor having a wide and direct bandgap (as wide as 3.37 eV), equivalent to that of GaN [5]. Besides this, ZnO is piezoelectric and optically transparent with a large exciton binding energy of 60 MeV.

In recent past, room-temperature (RT) ferromagnetism (FM) in transition metal (TM)-doped p-type ZnO has been repeatedly predicted by several groups using various calculations/simulation studies [6,7]. This makes ZnO one of the most promising materials for potential applications in spintronics and as diluted magnetic semiconductor (DMS) material. At the same time, besides theoretical predictions, RT FM in TM-doped ZnO has been reported by various experimentalists. Progress in producing high-quality ZnO to obtain ferromagnetism at or above room temperature by doping with 3d transition metals has been highlighted in several papers [8–11]. It has been found that the diluted magnetic semiconductors (DMSs) formed by replacing the cations of III–V or II–VI nonmagnetic semiconductors by ferro-

magnetic Mn, Fe, Co and Ni exhibit a number of unique magnetic, magneto-optical and magnetotransport properties, applicable for magneto-electronic and spintronic devices. Most of these studies focused on Mn- and Fe-doped ZnO films, while fewer studies on Ni-doped ZnO films have been reported [12]. The origin of RT FM in TM-doped ZnO are sensitive to the synthesis conditions, and are still debatable, thus, research work in this field is still in its infancy and stalk of RT FM semiconductors, which are the foundation for spintronics, are still exigency. Moreover, it also seems that most studies focus on film materials, and ferromagnetism could usually only be found in film materials. In the present paper, we reveal a simple technique to synthesize ZnO:Ni²⁺ nanoparticles with excellent structural and magnetic properties.

2. Experimental details

For synthesis of ZnO:Ni²⁺ nanoparticles, the zinc acetate dihydrate (99.2%) Zn(CH₃COO)₂·2H₂O, nickel acetate 1-hydrate (99.4%) (CH₃COO)₂Ni·H₂O, potassium hydroxide KOH, citric acid, methanol and ethanol were procured from E. Merck Limited, India. All chemicals were of analytical reagent grade and were directly used without any special treatment.

Synthesis of ZnO:Ni²⁺ nanoparticles were carried out using the same technique followed by us [11,13] for the synthesis of ZnO:Fe and ZnO:Cu nanoparticles. For synthesizing ZnO:Ni²⁺, 0.5 M of zinc acetate and 0.01 M of nickel acetate were taken in 100 ml of methanol and dissolved with continuous stirring for 2 h at room

* Corresponding author. Tel./fax: +91 532 2460675.

E-mail address: prashantnac@gmail.com (P.K. Sharma).

temperature (solution A). Simultaneously, 140 mmol KOH solution was prepared in 100 ml of methanol with refluxing through water condenser with constant stirring for 2 h at 50 °C (solution B). Now, mix the solution A and B with constant stirring for 2 h. This mixing was done while refluxing through water condenser at 50 °C. Final solution was allowed to cool at room temperature and aged overnight. This solution was centrifuged and washed several times with absolute ethanol and water in order to remove unnecessary impurities. The obtained white product was placed in a vacuum oven for 24 h at 50 °C to get white powders of ZnO:Ni²⁺. Similar procedure was followed for synthesis of ZnO:Ni²⁺ with varying Ni²⁺ doping percentage, i.e. 1%, 2%, 3%, 5%, 8%, 10%, 15% and 20% named as RNi 1, RNi 2, RNi 3, RNi 4, RNi 5, RNi 6, RNi 7 and RNi 8, respectively.

2.1. Characterization used

The prepared ZnO:Ni²⁺ nanoparticles were characterized by X-ray diffraction (XRD), transmission electron microscopy (TEM) and energy-dispersive X-rays (EDX), in order to elaborate structural properties in a precise manner for various doping percentage of Ni. XRD was performed on Rigaku D/max-2200 PC diffractometer operated at 40 kV/20 mA, using CuK_{α1} radiation with wavelength of 1.54 Å in the wide angle region from 25° to 70° on 2θ scale. The size and morphology of prepared nanoparticles were found using a transmission electron microscope (model Technai 30 G² S-Twin electron microscope) operated at 300 kV accelerating voltage by dissolving the as-synthesized powder sample in ethanol and then placing a drop of this dilute ethanolic solution on the surface of copper grid. Room-temperature magnetization measurement was carried out using a vibrating sample magnetometer (VSM, ADE Magnetics, USA) with pressed pellets of prepared powdered samples. Raman spectra were taken with a Reinshaw micro-Raman spectroscope using 514 nm Ar⁺ laser as excitation source.

3. Results and discussion

Fig. 1 shows the XRD pattern of the ZnO:Ni²⁺ nanoparticles synthesized in the current work. XRD spectra show broad peaks at

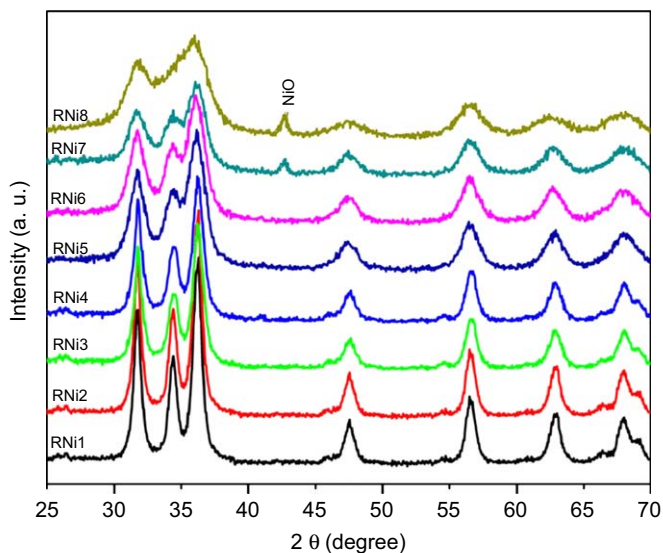


Fig. 1. X-ray diffraction spectra of ZnO for different doping percentage of Ni. The XRD spectra showed crystalline nature having hexagonal wurtzite structure of ZnO having space group P6_{3mc}. An additional peak, corresponding to NiO (200) phase was observed at 43.23°.

the positions of 31.63°, 34.50°, 36.25°, 47.50°, 56.60°, 62.80°, 66.36°, 67.92° and 68.91°, which are in good agreement with the standard JCPDS file for ZnO (JCPDS 36-1451, $a = b = 3.249$ Å, $c = 5.206$ Å) and can be indexed as the hexagonal wurtzite structure of ZnO having space group P6_{3mc}. Furthermore, it can be seen that at higher doping percentages of Ni²⁺ (15% and 20% in present case), a new phase emerges at 43.23° in the XRD spectra. This new phase in the XRD spectra corresponds to NiO (200) (matched with JCPDS 78-0643), which may be due to the formation of NiO from remaining un-reacted Ni²⁺ ions present in the solution. All the available reflections of the present XRD phases have been fitted with Gaussian distribution. The broadening of XRD peaks (i.e. Scherrer's broadening) attributes nanosized formation of ZnO:Ni²⁺. The particle size, d , of ZnO:Ni²⁺ nanoparticles were estimated by Debye–Scherrer's equation

$$d = \frac{0.9\lambda}{B \cos \theta}$$

where, d is the particle size, λ the wavelength of radiation used, θ the Bragg angle and B is the full-width at half-maxima (FWHM) on 2θ scale. The crystallite size was estimated for the strongest X-ray diffraction, corresponding to (002) peak at 36.25°, and was found to vary from 12 to 2 nm for samples RNi1–RNi8.

XRD pattern not only showed decreasing crystallite size for increasing doping percentage of Ni²⁺, but a significant degradation in crystallinity with enhanced peak broadening was also observed with increasing Ni²⁺ doping. Moreover, it can also be seen that as the Ni doping percentage increases, the wurtzite structure of ZnO starts gradual degradation. The degradation in crystallinity was observed from sample RNi 1–RNi 8 and enhancement in the peak broadening was also observed indicating more nano-nature of the higher Ni content samples. This was due to distortion in the host ZnO lattice, because of the introduction of a foreign impurity i.e. Ni doping. This is mainly because of decrease in nucleation and subsequent growth rate due to increasing Ni doping percentage due to the size difference of Zn and Ni ions. Ionic radius of Ni²⁺ is 0.68 Å and is larger than that of Zn²⁺ i.e. 0.60 Å and lowers the reaction rate.

The variations in XRD results were well supported by TEM measurements. Fig. 2 shows the representative TEM image of the prepared samples. The morphology of all the samples was found to be spherical in nature having diameters ranging from 15 to 3 nm for different samples. Fig. 2 clearly shows that the diameters of these spherical nanoparticles were in agreement with those obtained using XRD results. Fig. 2(f) shows the representative selected area electron diffraction (SAED) pattern for sample RNi 1, i.e. 1% Ni-doped ZnO samples. This SAED pattern showed that the prepared ZnO nanoparticles were polycrystalline in nature. Figs. 2(g) and 2(h) show high-resolution transmission electron microscopic (HRTEM) images of RNi 1 and RNi 8 samples, respectively. The imaged lattice spacing 2.3 Å (Fig. 2(g)) for RNi 1 (1% Ni) sample, corresponds to the (002) planes of hexagonal wurtzite structure of ZnO while a remarkable deviation in the imaged lattice spacing 2.16 Å (Fig. 2(h)) was observed for RNi 8 (20% Ni) sample. HRTEM measurements showed a remarkable shrink in imaged d -spacing for higher doping percentage of Ni (samples RNi 7 and RNi 8), whereas for the other samples no significant change in imaged d -spacing were observed as compared to standard ZnO wurtzite structure i.e. the effect of Ni doping is dominant and appeared only at higher doping percentages which is in good agreement with XRD, Raman and VSM results (to be discussed later on). This result further supported our claim that this distortion in the host ZnO lattice arises due to the introduction of a foreign impurity i.e. Ni²⁺ doping at higher doping percentage. Again the origin of this distortion in

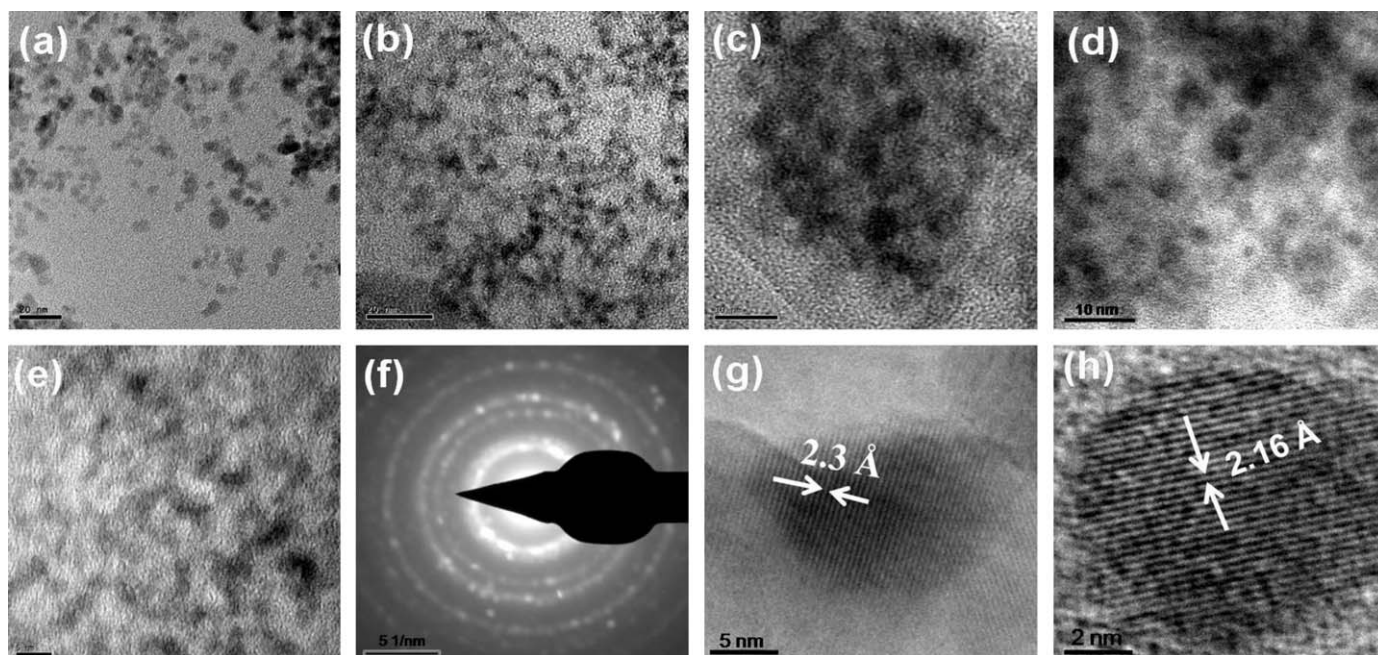


Fig. 2. Representative TEM images of ZnO:Ni nanoparticles, for sample RNi 1(a), RNi 2(b), RNi 4(c), RNi 6(d), RNi 8(e), respectively, (f) represents the SAED pattern for sample RNi 1. Representative HRTEM images of ZnO:Ni nanoparticles, for sample (g) RNi 1 and (h) RNi 8, respectively.

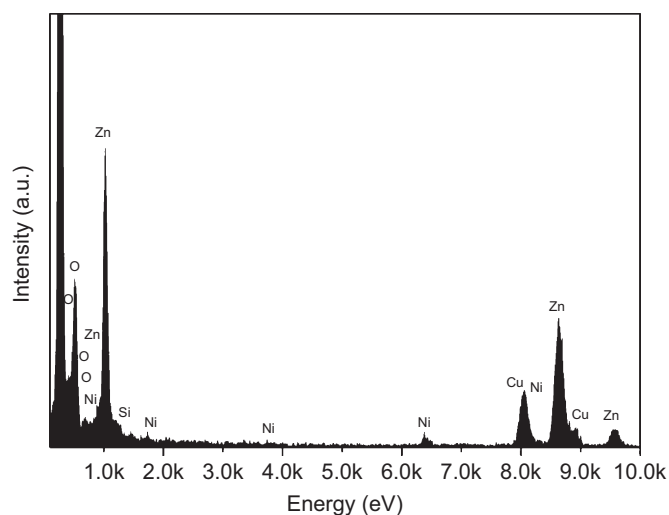


Fig. 3. Representative EDX spectra of RNi 2 sample, i.e. 2% Ni-doped samples. EDX measurements on single nanoparticle found that zinc and nickel are homogeneously distributed throughout the ZnO:Ni²⁺ nanoparticles.

host ZnO lattice could be attributed to the size difference of ionic radius of both Zn²⁺ and Ni²⁺ ions as discussed earlier.

In order to confirm the presence of Ni²⁺ in the synthesized ZnO nanoparticles, EDX measurements were performed. Fig. 3 shows the representative EDX spectra of RNi 2 sample, i.e. 2% Ni-doped samples. From the similarity of the Zn and Ni peak intensity line traces, it is clear that after the synthesis process, zinc and nickel were homogeneously distributed inside the nanoparticle. From the EDX line traces it can also be concluded that Ni²⁺ was successfully substituted into the crystal structure of ZnO nanoparticles. The estimated amount of Ni²⁺ ions were nearly 2%. EDX measurements on single ZnO:Ni²⁺ nanoparticles found that zinc and nickel were homogeneously distributed throughout the whole nanoparticle.

The presence of Cu line traces in EDX spectra could be attributed due to the signal arising from the copper grid used for the measurement. Fig. 4 shows the dependence of magnetization at room temperature with applied magnetic field (*M-H* loop) for sample (a) RNi 2 i.e. 2% Ni doping, (b) RNi 4 i.e. 5% Ni doping, (c) RNi 6 i.e. 10% Ni doping and (d) RNi 8 i.e. 20% Ni doping, respectively.

A clear hysteresis loop, with noticeable coercivity, was observed. Initially, ferromagnetic nature was observed for 1–5% Ni (RNi 1–RNi 4)-doped samples and again for further high doping of Ni (RNi 4–RNi 8) paramagnetic nature dominates. Initially, these nanoparticles showed strong ferromagnetic behavior, however, at higher doping percentage of nickel the ferromagnetic behavior was suppressed and paramagnetic nature was observed. The enhanced antiferromagnetic interaction between neighboring Ni–Ni ions suppressed the ferromagnetism at higher doping concentrations of Ni.

Clear hysteresis loops with coercivities 12.0, 10.2, 1.2 and 0.8 mT were observed for RNi 2, RNi 4, RNi 6 and RNi 8 samples, respectively. Their corresponding magnetizations of remanence were 10.1×10^{-3} , 9.8×10^{-3} , 7.28×10^{-3} and 5.92×10^{-3} emu/g, respectively. The noticeable coercivity of *M-H* loop could be attributed to strong ferromagnetism at room temperature. The narrow hysteresis implies a small amount of dissipated energy in repeatedly reversing the magnetization that is important for quick magnetization and demagnetization of the samples synthesized. The ferromagnetic behavior can be attributed to the presence of small magnetic dipoles located at the surface of nanocrystals, which interacts with their nearest neighbors inside the crystal. Consequently, the interchange energy in these magnetic dipoles making other neighboring dipoles oriented in the same direction. In nanocrystals, surface-to-volume ratio increases, so the population of magnetic dipoles oriented in the same direction will increase at the surface. Thus, the sum of the total amount of dipoles oriented along the same direction will increase subsequently. In short, the crystal surface will be usually more magnetically oriented.

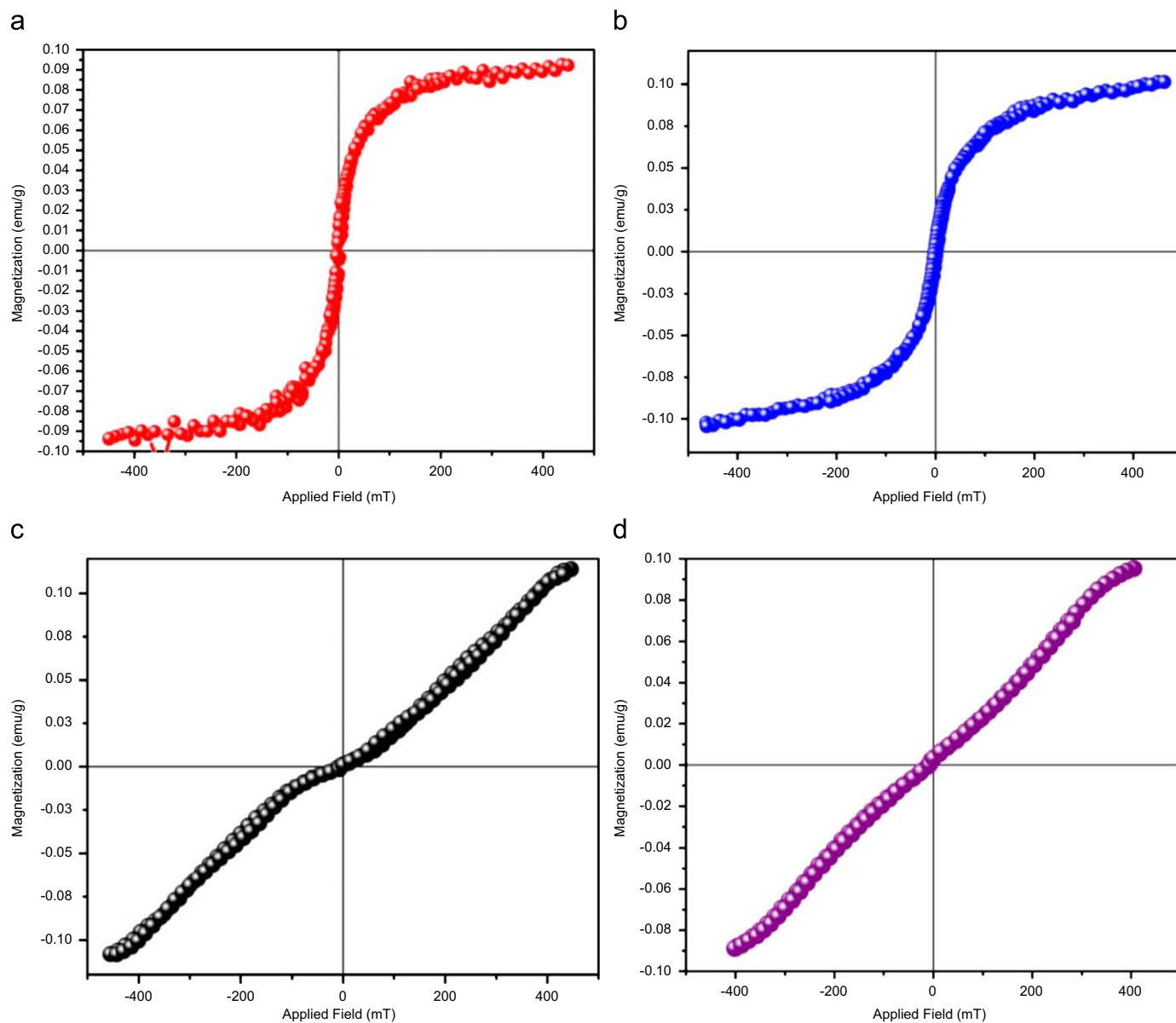


Fig. 4. Room-temperature $M-H$ loop for as-synthesized ZnO:Ni nanoparticles. (a) For RNi 2, i.e. 2%, (b) for RNi 4, i.e. 5%, (c) for RNi 6, i.e. 10% and (d) for RNi 8, i.e. 20% Ni-doped samples, Observed clear hysteresis indicates ferromagnetic nature of the prepared nanoparticles at room temperature.

Raman spectroscopic studies were employed to understand the effect of nickel doping on microscopic structure and vibrational properties of prepared ZnO:Ni²⁺ nanoparticles. Several literature show that in hexagonal wurtzite ZnO following fundamental optical bands should exist, as according to the group theory: E_2 (low) at 101 cm^{-1} , E_2 (high) at 437 cm^{-1} , A_1 (TO) at 380 cm^{-1} , A_1 (LO) at 574 cm^{-1} , E_1 (TO) at 407 cm^{-1} and E_1 (LO) at 583 cm^{-1} . The low-frequency E_2 mode is associated with the vibration of heavy Zn sub-lattice and the high-frequency E_2 mode involves only the oxygen atoms. Raman Spectra (Fig. 5) showed a strong Raman shift signal at $\sim 437\text{ cm}^{-1}$, which is due to E_2 (high) mode of ZnO nanoparticles. These results were consistent with already reported works [14–17]. The second-order vibrations were at 208 , 334 and $1050\text{--}1200\text{ cm}^{-1}$. Presence of small peak at ~ 583 and 378 cm^{-1} confirmed that oxygen deficiency is quite low in the nickel-doped ZnO and are due to E_1 (LO) and A_1 (TO) modes of ZnO, respectively, this peak diminishes gradually with increasing concentration of Ni, the dopant. The other peaks appearing in the low-frequency region corresponds to the

second-order vibration modes of ZnO. These results further confirm that the ZnO:Ni²⁺ nanoparticles are composed of hexagonal wurtzite structure. Some other peaks at positions 1347 and 1426 cm^{-1} , were also observed for higher doping percentage of nickel.

For RNi 1 sample, very strong and sharp Raman peaks were observed, indicating good wurtzite structure. The sharpest and strongest peak at about 437 cm^{-1} is the strongest Raman mode in wurtzite crystal structure. However, as the Ni content increases to 5% and above, the Raman line of E_2 (high) mode becomes broad and weak, which means that the wurtzite crystalline structure of ZnO might have been weakened by higher Ni doping concentration. It is well known that lattice defects and disorder could usually be introduced by exotic ions doping, defect-induced Raman modes would usually appear in defective crystals because the Raman selection rules are relaxed [18]. For high-concentration-doped crystal, the translational invariance of the crystal lattice is weakened and scattering events from the whole Brillouin zone are possible.

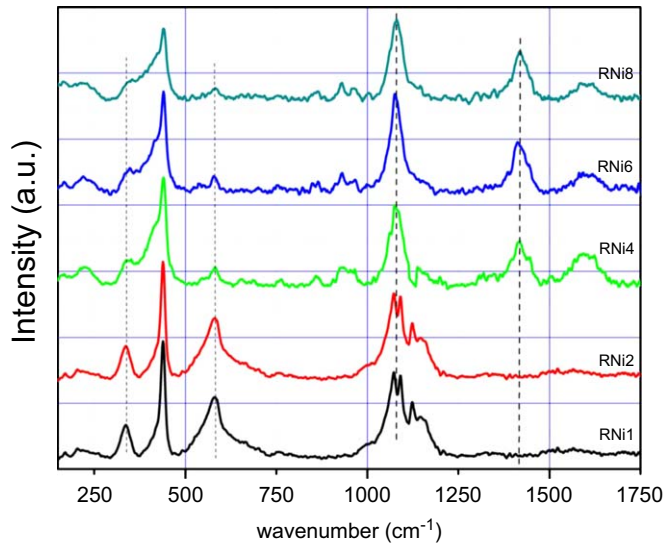


Fig. 5. Representative Raman spectra of ZnO:Ni²⁺ nanoparticles with various doping percentage of nickel.

4. Conclusion

We have successfully synthesized the ultrafine diluted magnetic semiconductors nanoparticles of ZnO:Ni²⁺ of mean size 212 nm at room temperature. XRD analysis and Raman study show wurtzite structures for all the ZnO:Ni²⁺ nanoparticles. With increasing Ni concentration, the wurtzite structures degrade gradually. Initially, these nanoparticles showed strong ferromagnetic behavior, however, at higher doping percentage of Ni the ferromagnetic behavior was suppressed and paramagnetic nature was observed. The enhanced antiferromagnetic interaction be-

tween neighboring Ni–Ni ions suppressed the ferromagnetism at higher doping concentrations of nickel.

Acknowledgements

Authors are thankful to DST and CSIR, India for the financial assistance during the current work. Prof. S.C. Kashyap at IIT Delhi is thankfully acknowledged for the VSM measurements of all the samples.

References

- [1] S.M. Prokes, K.L. Wang, *Mater. Res. Sci. Bull.* 24 (1999) 13.
- [2] J. Hu, T.W. Odom, C.M. Lieber, *Acc. Chem. Res.* 32 (1999) 435.
- [3] S. Nakamura, *Science* 281 (1998) 956.
- [4] C.A. Mirkin, *Science* 286 (1999) 2095.
- [5] V.A. Karpina, V.I. Lazorenko, C.V. Lashkarev, V.D. Dobrowolski, L.I. Kopylova, V.A. Baturin, S.A. Lytuyn, V.P. Ovsyannikov, E.A. Mauvenko, *Cryst. Res. Technol.* 39 (2004) 980–992.
- [6] T. Dietl, H. Ohno, F. Matsukura, J. Cibert, D. Ferrand, *Science* 287 (2000) 1019.
- [7] M.H.F. Sluiter, Y. Kawazoe, P. Sharma, A. Inoue, A.R. Raju, C. Rout, U.V. Waghmare, *Phys. Rev. Lett.* 94 (2005) 187204.
- [8] S.J. Pearton, D.P. Norton, K. Ip, Y.W. Heo, T. Steiner, *J. Vac. Sci. Technol. B* 22 (2004) 932.
- [9] C. Liu, F. Yun, H. Moroc, *J. Mater. Sci.* 16 (2005) 555.
- [10] R. Janisch, P. Gopal, N.A. Spaldin, *J. Phys.: Condens. Matter* 17 (2005) R657.
- [11] P.K. Sharma, R.K. Dutta, A.C. Pandey, S. Layek, H.C. Verma, *J. Magn. Magn. Mater.* 321 (2009) 2587.
- [12] G.J. Huang, J.B. Wang, X.L. Zhong, G.C. Zhou, H.L. Yan, *J. Mater. Sci.* 42 (2007) 6464–6468.
- [13] P.K. Sharma, R.K. Dutta, M. Kumar, P.K. Singh, A.C. Pandey and V.N. Singh, *IEEE TNANO*, article in press, (2009), Article ID: TNANO-00111–2009.
- [14] Z. Wang, H. Zhang, L. Zhang, J. Yang, S. Yan, C. Wang, *Nanotechnology* 14 (2003) 11.
- [15] T.C. Damen, S.P.S. Porto, B. Tell, *Phys. Rev.* 142 (1996) 570.
- [16] Z. Zhang, B. Huang, Y. Yu, D. Guo, *Mater. Sci. Eng. B* 86 (2001) 109.
- [17] M. Koyano, P. Quoc Bao, L.T. ThanhBinh, H.L. Hong, N. Ngoc Long, S.I. Katayama, *Phys. Staus Solidi A* 193 (2002) 125.
- [18] A. Chartier, P.D. Arco, R. Dovesi, V.R. Saunders, *Phys. Rev. B* 60 (1999) 14042.